Origin of Simultaneous Donor−Acceptor Emission in Single Molecules of Peryleneimide−Terrylenediimide Labeled Polyphenylene Dendrimers

Sergey M. Melnikov,[†] Edwin K. L. Yeow,[‡] Hiroshi Uji-i,[†] Mircea Cotlet,[§] Klaus Müllen,[||] Frans C. De Schryver,[†] Jörg Enderlein,[⊥] and Johan Hofkens*,[†]

Department of Chemistry, Katholieke Universiteit Leuven, Celestijnenlaan 200 F, 3001 Heverlee, Belgium, Division of Chemistry and Biological Chemistry, Nanyang Technological University, 1 Nanyang Walk, Block 5, Level 3, Singapore 637616, Physical Chemistry and Applied Spectroscopy, Los Alamos National Laboratory, Mail Stop J576, Los Alamos, New Mexico 87545, Max-Planck-Institut für Polymerforschung, Ackermannweg 10, 55128 Mainz, Germany, and Institute for Biological Information Processing I, Forschungszentrum Jülich, D-52425 Jülich, Germany

Received: August 28, 2006; In Final Form: October 20, 2006

Förster type resonance energy transfer (FRET) in donor−acceptor peryleneimide−terrylenediimide dendrimers has been examined at the single molecule level. Very efficient energy transfer between the donor and the acceptor prevent the detection of donor emission before photobleaching of the acceptor. Indeed, in solution, on exciting the donor, only acceptor emission is detected. However, at the single molecule level, an important fraction of the investigated individual molecules (about 10−15%) show simultaneous emission from both donor and acceptor chromophores. The effect becomes apparent mostly after photobleaching of the majority of donors. Single molecule photon flux correlation measurements in combination with computer simulations and a variety of excitation conditions were used to determine the contribution of an exciton blockade to this two-color emission. Two-color defocused wide-field imaging showed that the two-color emission goes hand in hand with an unfavorable orientation between one of the donors and the acceptor chromophore.

1. Introduction

In recent years, a lot of research has been devoted to the development of photoactive dendrimers, that is, dendrimers containing one type of chromophore in the core or several different types of chromophores positioned throughout the dendritic structure: in the core, in the dendritic arms, or at the rim.[1] This development is driven not only by the synthetic challenge[2] but also by the fact that this type of molecules can serve as model compounds for the study of fundamental photophysical processes occurring in natural light harvesting systems. Energy hopping has been demonstrated by decorating dendrimers with one type of chromophore at the rim.[3] Directional energy transfer, both in the weak and strong coupling regimes, has been studied by introducing a gradient from the rim or branches toward the core of the dendrimer.[4−6] Dendrimers have been developed that showed a cascade and/or stepwise Förster type energy transfer.[7,8] Another key process of photosynthesis, electron transfer, has also been studied in specially tailored dendrimers.[9−12] Recently, a dendrimer showing energy transfer followed by electron transfer from the core was reported.[13]

The main advantage of using dendrimers for the study of fundamental photophysical processes is the control that can be obtained over the number of chromophores, the distance between them, and even the orientation between energy/electron donors−acceptors. By looking at such dendritic systems at the single molecule level, both at room temperature and at cryogenic temperatures, an even more detailed picture of the complex photophysics in such systems under high photon fluxes can be obtained. Single molecule spectroscopy of dendrimers, owing to sensitivity of this approach to spatial and temporal heterogeneity of the examined system, allows observation and quantification of photophysical processes that are rather difficult to access in ensemble measurements. Indeed, processes such as singlet−singlet annihilation or singlet quenching by a triplet (singlet−triplet annihilation) have been observed.[10,14] Different energy transfer pathways within one dendrimer molecule have been unraveled.[8,15] Furthermore, the role of higher excited state processes has been proven and quantified.[16] In the case of electron transfer at the single molecule level, changes in the rate constant of transfer have been observed and attributed to libration motions in the dendrimer.[9,10] All phenomena described above are relevant for and have been seen in other multichromophoric architectures such as conjugated polymers, natural antenna systems, and self-assembled nano-objects.[17]

A particular well studied system at the ensemble and single molecule level is the first (**T1P$_4$**) and second (**T2P$_8$**) generation of a structurally well-defined polyphenylene dendrimer consisting of four or eight peripheral perylenemonoimide (PI) chromophores which serve as an energy donor and a central terylendiimide (TDI) which acts as an energy acceptor.[18] Due to the large overlap between the emission spectrum of PI and the absorption spectrum of TDI, the efficiency of energy transfer is nearly unity in both generations of the dendrimer. This means that every excited donor chromophore transfers its energy completely to the acceptor chromophore, resulting in virtually no detectable donor emission. However, under conditions of

* To whom correspondence should be addressed. Phone: + 32-16-327804. Fax: +32-16-327990. E-mail: Johan.Hofkens@chem.kuleuven.be.
[†] Katholieke Universiteit Leuven.
[‡] Nanyang Technological University.
[§] Los Alamos National Laboratory.
[||] Max-Planck-Institut für Polymerforschung.
[⊥] Institute for Biological Information Processing I.

10.1021/jp0655625 CCC: $37.00
Published on Web 01/06/2007

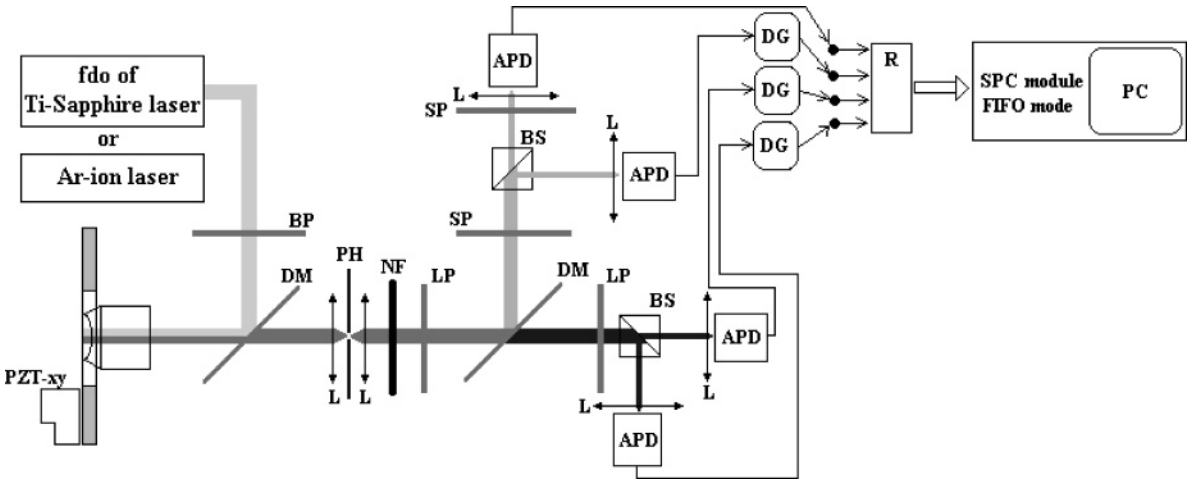

Figure 1. Schematic of the confocal microscopy setup: BP, band-pass filter; PZT-xy, piezoelectric stage; DM, dichroic mirror; PH, pinhole; NF, notch filter; LP, long-pass filter; BS, beam splitter; SP, short-pass filter; L, lens; APD, avalanche photodiode; GD, electronic delay generator; R, router; PC, computer; SPC module FIFO mode: single photon counting module operated in first in, first out mode.

high photon flux, even for donor−acceptor pairs that allow for very efficient energy transfer, sometimes donor emission can be observed.[6,8] This unexpected donor emission is said to result from a so-called "exciton blockade" and is attributed to the presence of multiple excitations. When several excited donors are simultaneously present within one macromolecule, one of them will transfer its energy to the acceptor. As long as the acceptor is in the excited state, energy transfer from the other donors will be prohibited or blocked and as a result they can in principle relax to the ground state via fluorescence. Since the excited state lifetimes of PI and TDI are comparable, this should result in nearly simultaneous donor and acceptor emission. At high excitation power, single molecules of peryleneimide−terrylenediimide dendrimers indeed displayed two-color emission.[6] Hence, this observation was tentatively attributed to the exciton blockade described above. An appearance of this effect also for single pairs of dye molecules (Cy3 and Cy5) coupled by Förster type resonance energy transfer (FRET) has been lately surmised.[19]

In this contribution, we direct our attention to this two-color fluorescence observed for individual molecules of the donor and acceptor labeled polyphenylene dendrimers described above in order to obtain an in-depth understanding of the mechanisms responsible for this phenomenon. Two-color confocal single molecule detection as well as two-color defocused wide-field detection in combination with numerical calculations and Monte Carlo simulations have been applied.

Throughout this paper, we will use the terms "red emission" and "green emission" to designate fluorescence of the TDI chromophore (710 nm emission maximum) and the PI chromophore (570 nm emission maximum), respectively. Also, we will call the PI chromophore the energy donor and the TDI chromophore the energy acceptor, the FRET process from PI donors to the central TDI acceptor directional FRET, and the energy transfer process between identical chromophores (PI chromophores in our case) energy hopping.

2. Experimental Section

Immobilization of single molecules was done by spin coating, at 2000 rpm, a chloroform solution of 5 mg/mL Zeonex (polynorbornene) containing 10^{-10} M of the dendrimers on a glass cover slip. The film thickness is approximately 100−200 nm in this case with single dendrimers dispersed in the film. Their density was evaluated to be around 0.1−0.2 μm^{-2}.

The confocal microscopy setup operating in the epiluminescence regime is displayed in Figure 1 (it was reported elsewhere in detail[20]). Photoexcitation sources are the 488 nm line of a continuous wave (CW) Ar-ion laser (Stabilite, Spectra-Physics) and the frequency doubled, pulse picked output of a Ti−sapphire laser (Tsunami, Spectra-Physics, 8.18 MHz after pulse picking, 1.2 ps fwhm). The laser light passing through a 488 nm band-pass filter is focused on the sample by an oil immersion objective (Olympus, 1.4 N.A., 60×). Fluorescence is collected by the same objective and separated from scattered excitation light by a dichroic mirror (DRLP490 Omega filter) and subsequently focused onto a pinhole for confocal detection. After recollimation, the emitted beam is cleaned up with a notch filter (Kaiser Optics) and a 515 nm long-pass filter and then divided by a second dichroic mirror (DRSP630 Omega filter) into two color channels, one corresponding to the donor emission (maximum 560 nm) and one corresponding to the acceptor emission (maximum 705 nm). In each channel, a 50/50 nonpolarizing beam splitter further divides the signal into two parts, which are then focused onto the sensitive area of an avalanche photodiode (APD, EG&G). In addition, fluorescence in the donor and accepter channels is filtered by a short-pass 600 nm filter and a long-pass 690 nm filter, respectively. Furthermore, to suppress parasitic cross-talk ("after glow") due to photons generated by a detection event of the other avalanche photodiode, a 700 nm short-pass filter is inserted in front of one of the detectors of the donor detection channel.[21] We measured the fluorescence intensity (number of photons) and the temporal coordinates of the photocounts with respect to the excitation pulse, simultaneously, by single photon counting (SPC) PC cards (SPC 630 Becker-Hickl) operating in the FIFO (first in, first out) mode. Electronic delay generators (Stanford Research DG535) were placed in three detection channels to avoid SPC-card dead-time distortions.

The wide-field fluorescence microscopy setup is shown in Figure 2 (it has been recently reported in detail[22]). It includes an optical microscope equipped with an oil immersion objective (Plan Fluorite, Olympus, 1.3 N.A., 100×) and a highly sensitive CCD camera (Cascade 512B, Roper Scientific). The excitation source is the 488 nm line of a continuous wave (CW) Ar-ion laser (Stabilite, Spectra-Physics). Wide-field illumination is achieved by focusing the expanded and collimated laser beam onto the back-focal plane of the objective. The polarization of excitation light in the sample plane was cautiously tuned to be

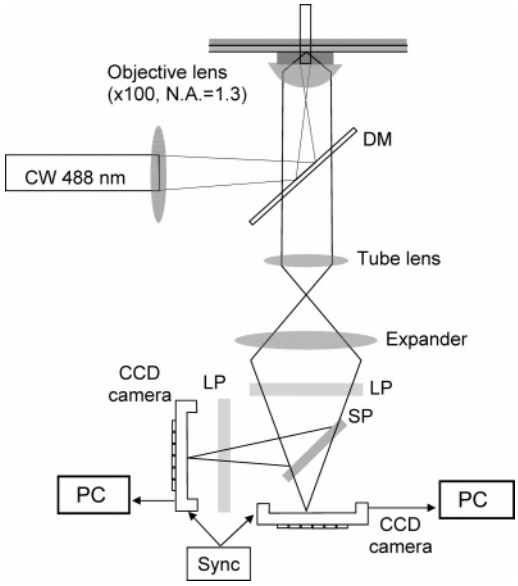

Figure 2. Schematic of the wide-field fluorescence microscopy setup: SP, short-pass filter; LP, long-pass filter; DM, dichroic miror; PC, personal computer; Sync, synchronization unit.

circular using zero-order $\lambda/4$ and $\lambda/2$ waveplates to compensate for polarization effects of the dichroic mirror. Fluorescence is collected by the same objective and separated from scattered excitation light by a dichroic mirror. Then, the expanded light beam is filtered by a long-pass 500 nm filter. Next, the fluorescence is divided by a short-pass 650 nm filter (mounting at an angle of 45° with respect to the optical axis) into donor and acceptor emission. Donor and acceptor fluorescence are imaged on two synchronized CCD cameras after magnification with a 3.3× camera lens. In addition, fluorescence in the accepter channels is filtered by a 690 nm long-pass filter. An external TTL single pulse generator is used to synchronize the CCD cameras. To obtain the defocused images, the sample is positioned by ~1 μm toward the microscope objective from the focus using a piezoelectric transducer (PI5173C1, Physik Instrumente). The integration time per frame was set to 1 s. The duration of measurement was 1500 s. Measurements were always carried out at ambient temperature and atmosphere. Data are processed using the so-called BIFL data analyzer software (in-house-developed software)[23] and in MATLAB.

3. Simulations and Calculations

3.1. The Use of Correlation Functions for Unraveling the Origin of the Two-Color Emission. In order to prove if an exciton blockade is the source of the two-color emission in T1P4 and T2P8, one can look at the correlation between the donor and acceptor photons. As argued in the Introduction, due to the similar excited state lifetimes of the PI and TDI chromophore, in the case of an exciton blockade, the green and red photons should be correlated. Correlation functions are often used to examine the statistical dependence of a process or the statistical dependence between two (random) processes. The intensity correlation function, $g^{(2)}(\tau)$, of two photon streams (for *stationary* processes, i.e., $\langle I(t)\rangle$ is a constant value) is defined as

$$g^{(2)}(\tau) = \frac{\langle I_i(t)\, I_j(t+\tau)\rangle_t}{\langle I_i(t)\rangle_t \langle I_j(t)\rangle_t} \qquad (1)$$

For the case when $i = j$, $g^{(2)}(\tau)$ is an autocorrelation function, and when $i \neq j$, it is a cross-correlation function. Under pulsed excitation, the correlation function displays a series of peaks separated by the pulse repetition interval ($\Delta t = 122$ ns for the pulsed laser used). In the remainder of the text, only three peaks will be considered: the "zero-time" peak ($\tau = 0$), the positive adjoining peak ($\tau = \Delta t$), and the negative adjoining peak ($\tau = -\Delta t$). Three cases of statistical dependence have been considered: thoroughly correlated photon fluxes, anticorrelated photon fluxes, and uncorrelated photon fluxes. In order to make our results comparable with experimental accessible photon coincidence measurements,[24,25] we simulated coincidence histograms, $C(\tau)$, which are proportional to the correlation function, $g^{(2)}(\tau)$:[26]

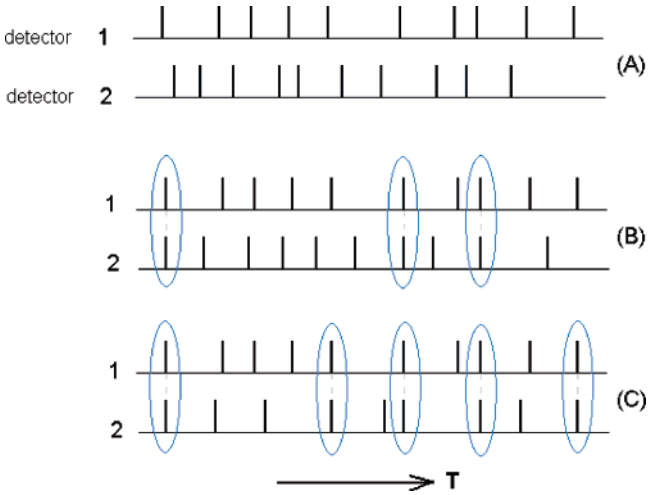

Figure 3. Photon arrival times of two detection channels: (A) anticorrelated photon steams; (B) uncorrelated photon streams; (C) correlated photon streams. Blue ovals plus gray dashed lines depict coincidence events. For case C, not all photons in the second channel coincide with those in the first because of detection efficiency restrictions.

$$C(\tau) = g^{(2)}(\tau) N^2/T \qquad (2)$$

where N is the total number of photons detected and T is the observation time duration. In our simulations, we do not take into account background photons and APD dark photons. Experimentally, the coincidence histograms are measured by splitting the fluorescence of a single photon source into two channels by a 50/50 beam splitter (Hanbury−Brown−Twiss type of setup[27]), and a fluorescence correlation function in the nanosecond time range can be constructed from the detected photons subsequently.[28]

Monte Carlo simulations were used to construct the coincidence histograms for each of the three cases outlined above. Data sets which mimic experimental single molecule fluorescence trajectories have been generated. For each laser pulse, separated in time by Δt, the emitted photon was considered to be detected successfully if a random number, $y \in [0;1]$, chosen from a uniform distribution was less than Pd, where P is the probability to emit a photon by a molecule (comprising the absorption cross section, photon flux, fluorescence quantum yield, and absorption dipole orientation) and d is the detection efficiency of the setup. The coincidence histograms are subsequently built by calculating the interphoton arrival times.

3.2. Anticorrelated Photon Sequences. In this case, the arrival of a photon in one channel excludes a simultaneous photon arrival in the other detection channel (i.e., it is impossible to detect photons in both channels at the same time). Figure 3A displays the photon arrival times of two anticorrelated photon sequences where there is no simultaneous detection of photons

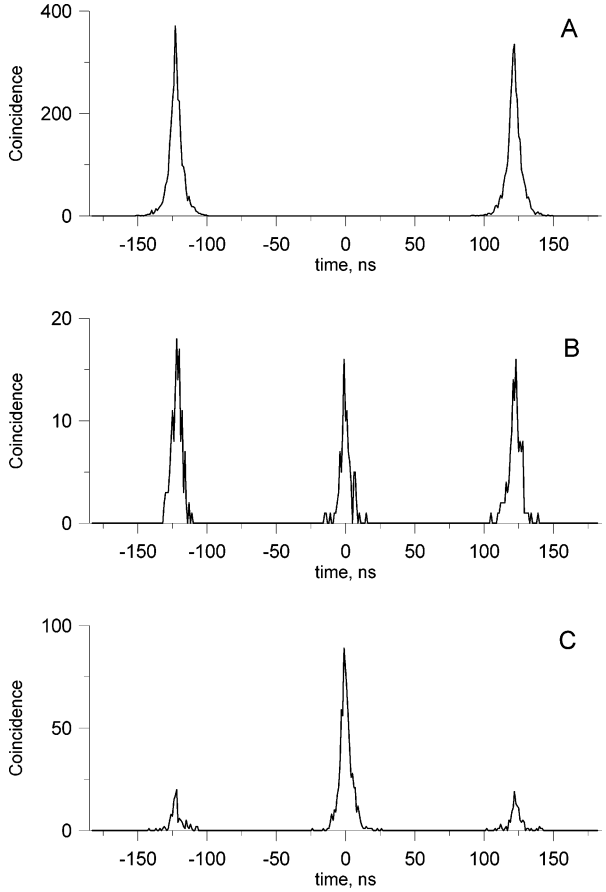

Figure 4. Simulated coincidence histograms: (A) Anticorrelated photon streams. The histogram was calculated from simulated traces, lasting 10 s, with a 5×10^4 cps rate. (B) Uncorrelated photon streams. The histogram was calculated from simulated traces, lasting 10 s, with a 1×10^4 cps rate. (C) Correlated photon streams. The histogram was calculated from simulated traces, lasting 20 s, the first trace with a 3.272×10^4 cps rate and the second with a 2.061×10^3 cps rate (the probability, p, to generate a photon in the second channel for each photon in the first stream is 0.063).

in both channels. Consequently, the autocorrelation histogram is characterized by the absence of a "zero-peak" (i.e., there is no coincidence at time $\tau = 0$). This statistical behavior of photon fluxes is called "photon antibunching" and serves as a signature of a single photon source, for example, a single chromophoric single molecule.[29] The Monte Carlo simulated coincidence histogram of two anticorrelated sequences is shown in Figure 4A.

3.3. Uncorrelated Photon Sequences. In this scenario, a photon in the first detection channel arrives independently from the arrival of a photon in the second detection channel and vice versa. Photon arrival times for this case are depicted in Figure 3B. The number of events where photons from both sequences are detected simultaneously occurs with the same frequency as that for photons separated in time by n ($n = 1, 2, 3, ...$) laser repetition periods, Δt, up to intervals of several microseconds. In principle, for an ideal case, the interphoton arrival time distribution decays exponentially with a parameter which is reciprocal to the count rate. Background photons, APD dark counts, and after-pulses truncate this distribution at longer times (longer than the sub-microsecond time range).

The Monte Carlo simulated coincidence histogram of two uncorrelated photon sequences is represented by a series of identical peaks (see Figure 4B), where the number of coincidence events, N_{un}, per peak is given by

$$N_{un} = (P_1 d_1)(P_2 d_2) LT \tag{3}$$

where $P_{1(2)}$ is the probability to generate a photon in the first (second) channel for a laser pulse, $d_{1(2)}$ is the detection efficiency of the first (second) channel, and L is the laser repetition rate. Equation 3 is valid for constant P_1 and P_2 during T. In general, N_{un} can also be expressed by

$$N_{un} = \frac{1}{L} \int_T R_1(t)\, R_2(t)\, \mathrm{d}t \tag{4}$$

where $R_{1(2)}(t)$ is the count rate for the first (second) detection channel.

3.4. Correlated Photon Sequences. For the sake of simplicity, we assume that each photon of one stream initiates a photon in another stream with probability ρ ($0 < \rho \leq 1$). This situation is to be expected if the simultaneous donor−acceptor fluorescence is resulting from an exciton blockade. Photon arrival times in this case are illustrated in Figure 3C, where the contribution of simultaneous photon detection events is higher than the contribution in uncorrelated photon sequences (Figure 3B). The coincidence histogram displayed in Figure 4C was calculated from Monte Carlo simulated time traces with a duration of 20 s and with 3.272×10^4 and 2.061×10^3 cps rates for detectors 1 and 2, respectively. The probability, ρ, for each photon in channel 1 to initiate a photon in channel 2 is 0.063. The number of events in the central peak, N_0, is given by

$$N_0 = P_1 \rho d_1 d_2 LT \tag{5}$$

Since $P_2 = P_1 \rho$, the ratio between the number of events in the adjoining (uncorrelated) peak, N_{adj}, and the central peak, N_0, is

$$\frac{N_{adj}}{N_0} = P_1 \tag{6}$$

In the case of $P_1 = 1$, the coincidence histogram will be similar to that for the uncorrelated photon sequences; however, this is not common, since a large excitation intensity is required.

Thus, the characteristic signatures of the different types of correlations should allow one to confirm if an exciton blockade is the origin of the observed simultaneous donor−acceptor emission. Note, however, that a coincidence histogram consisting of peaks of the same number of coincidences can also be obtained from a combination of anticorrelated and correlated sequences. If for each laser pulse a photon source generates a photon which appears in either channel 1 or channel 2 with probability p_{anti} and a pair of photons in both channels simultaneously with probability p_{corr}, the ratio N_{adj}/N_0 is determined from

$$\frac{N_{adj}}{N_0} = \frac{(p_{anti}/2 + p_{corr})^2}{p_{corr}} \tag{7}$$

3.5. Calculation of the Probability of Multiple Excitations in the Dendrimers. The concept of an exciton blockade relies on the fact that the multiple excitations can be generated in multichromophoric molecules within one excitation pulse. Here, we evaluate the probability of multiple excitations for the excitation power and laser pulses used in the experiments. The number of excited chromophores obtained during the course of a laser pulse was evaluated using the following formula

$$P_j^i = \sum^{C_j^i}\left(\prod_{k=1}^{j}\left(1 - \exp\left(-\frac{WA\xi_k}{L}\right)\right)\prod_{l\neq k}^{i-j}\exp\left(-\frac{WA\xi_l}{L}\right)\right) \quad (8)$$

where the sum runs over all possible combinations of j indices, P_j^i is the probability to excite j chromophores per laser pulse for a molecule comprising of i chromophores, $C_j^i = i!/[j!(i - j)!]$, W is the intensity of incident radiation expressed in photons/(cm^2 s) (e.g., for 488 nm laser light with an intensity of 2500 W/cm^2, $W \approx 6 \times 10^{21}$ photons/(cm^2 s)), L is the laser pulse repetition rate, A is the absorption cross section of the perylenemonoimide chromophore, and ξ_n is the transition dipole orientation factor of the nth chromophore with respect to the incident light. The probabilities to excite one, two, and three chromophores for a dendritic molecule containing eight, four, and two perylenemonoimide units per laser pulse were calculated for $\xi = 1$, and the results are listed in Table 1. To calculate P_j^i within a certain time interval, Δt, under CW excitation conditions, the value of $1/L$ in eq 8 has to be substituted by a value for Δt.

4. Results and Discussion

4.1. Bulk Measurements. The bulk spectroscopic properties of **T1P$_4$** and **T2P$_8$** and their constituting chromophores PI and TDI have been reported in several publications.[5] The molecular structures and the intramolecular distances between chromophores in **T1P$_4$** and **T2P$_8$** are displayed in Table 2 and Figure 5. Four types of intramolecular energy transfer processes which can occur in these dendritic systems have to be considered.

These processes are directional FRET, energy hopping, singlet (peryleneimide)−singlet (terrylenediimide) annihilation, and singlet (peryleneimide)−singlet (peryleneimide) annihilation. Figure 6 shows the different absorption and emission spectra that are relevant to these processes.[5] From the spectral overlap, Förster radii for the different processes can be calculated, and they are presented in Table 3. Note that for one important process, singlet PI−singlet TDI annihilation, the Förster radius was not available at the time of the previous publication dealing with exciton blockades.[6a] Although the Förster radius for PI−TDI annihilation, and hence the corresponding rate constant, is the smallest of all competing processes, it is still quite efficient in both generations of dendrimers. Assuming a random orientation between the chromophores involved in the process, the rate constant for PI−TDI annihilation, $k_{\mathrm{PI-TDIanni}}$, was calculated according to the following formula

$$k_{\mathrm{PI-TDIanni}} = k_{\mathrm{D}}\left(\frac{R_0}{r}\right)^6 \quad (9)$$

with $k_{\mathrm{D}} = 1/\tau_{\mathrm{D}}$ (2.5×10^8 s^{-1}) and with the Förster radius, R_0, and the intermolecular distance, r, values from Tables 2 and 3, respectively, to be 4.3×10^9 s^{-1} (for T1P$_4$) or 7.2×10^8 s^{-1} (for T2P$_8$). Hence, the rate constant of annihilation is always faster then the rate constant for fluorescence, meaning that most of the time the excited state on PI will disappear via annihilation rather then via fluorescence if excited PI and TDI chromophores are simultaneously present in the dendritic systems. These data give a first hint that an exciton blockade as such is not sufficient to explain the previously reported simultaneous donor−acceptor emission.

4.2. Confocal Single Molecule Microscopy. Fluorescence transients of 110 single molecules of **T1P$_4$** and 339 single molecules of **T2P$_8$** under pulsed excitation were analyzed. Furthermore, fluorescence traces of 66 single molecules of **T1P$_4$** and 95 single molecules of **T2P$_8$** were recorded using CW excitation. In order to compare with the data reported in ref 6, the same excitation power of 2.5 kW/cm^2 was used.

TABLE 1: Calculated Probability to Excite One, Two, and Three Chromophores During the Course of a Laser Pulse at a 2500 W/cm^2 Excitation Power for Molecules Comprising Two, Four, and Eight Donors

probability to excite:	molecule comprising: two chromophores	four chromophores	eight chromophores
one chromophore	0.191	0.304	0.387
two chromophores	0.012	0.054	0.163
three chromophores	0	0.004	0.038

TABLE 2: Intramolecular Distances

chromophore	compound	r (nm)
peryleneimide−terrylenediimide	**T1P$_4$**	2.3
	T2P$_8$	3.1
peryleneimide−peryleneimide	**T1P$_4$**	from 0.5 to 4
	T2P$_8$	from 0.5 to 5.5

The measured single molecules can be divided into three groups according to the appearance of the recorded fluorescence intensity traces: (1) molecules showing only red emission, (2) molecules showing red emission followed by green emission, and (3) molecules displaying two-color (i.e., simultaneous red and green emission during part of the trajectory) emission. Typical fluorescence trajectories of single molecules of type 1 and type 2, which display only monochromatic emission, are shown in Figure 7. The insets show the distribution of the fractional intensity, $F_{\mathrm{A}}(t)$, of the acceptor fluorescence

$$F_{\mathrm{A}}(t) = \frac{I_{\mathrm{A}}(t)}{I_{\mathrm{A}}(t) + I_{\mathrm{D}}(t)} \quad (10)$$

where $I_{\mathrm{A}}(t)$ and $I_{\mathrm{D}}(t)$ are the fluorescence intensity of the acceptor and the donor, respectively. Three fluorescence traces (A, C, and D) show first red emission followed by green emission after bleaching of the acceptor, and one (B) shows solely red fluorescence, in accordance with ref 18. Corresponding distributions of $F_{\mathrm{A}}(t)$ display two states of FRET efficiency: "zero" and "one", or only "one" for case B. Stepwise decrease of the fluorescence intensity has been attributed to successive reduction of the number of donors due to photobleaching.[18]

Two-color fluorescence traces (type 3) and corresponding distributions of $F_{\mathrm{A}}(t)$ are displayed in Figure 8. For these traces, distributions of $F_{\mathrm{A}}(t)$ present, besides zero and one FRET efficiency, a range of intermediate states. The dual-color fluorescence is registered only after significant decrease of acceptor emission from initial level. As stated above, this decrease in the acceptor emission intensity is attributed to sequential bleaching of donor chromophores.

The number of molecules found in each group under different excitation conditions and their corresponding relative contributions are summarized in Table 4. The majority of molecules fall into the first two groups as expected because of the very efficient directional energy transfer occurring in these systems. Nevertheless, approximately 10−15% of the traces show the simultaneous donor−acceptor emission. The relative contribution of each group is nearly equal for both dendrimer generations and for the different excitation conditions (pulsed versus CW excitation). The comparison between calculated multiexcitation probabilities (Table 1) with experimental data suggests against the exciton blockade as a main origin for the observed dual-

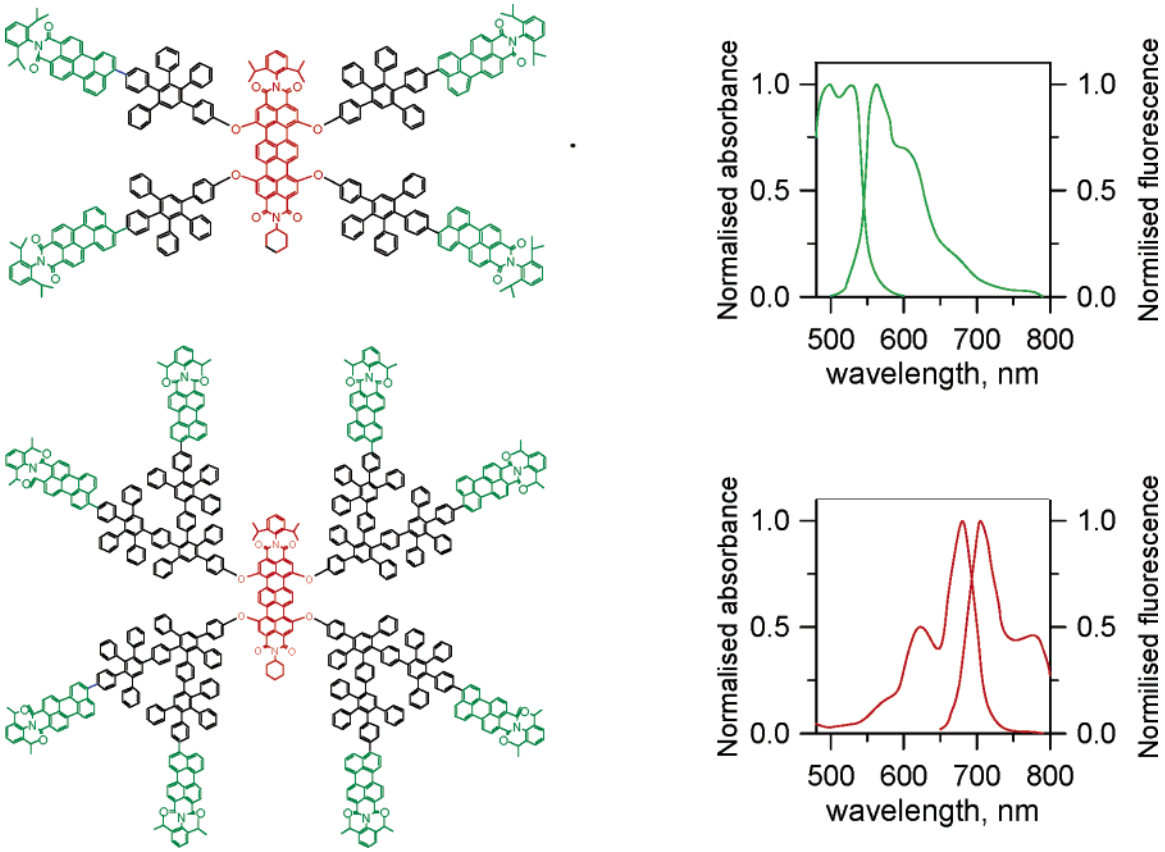

Figure 5. Structure of the compounds used in this study (upper left, **T1P$_4$**; lower left, **T2P$_8$**) and superimposed absorption and emission spectra for donor−acceptor chromophores PI−TDI (upper right, PI; lower right, TDI). Red and green colors denote terrylenediimide chromophores and peryleneimide chromophores correspondingly.

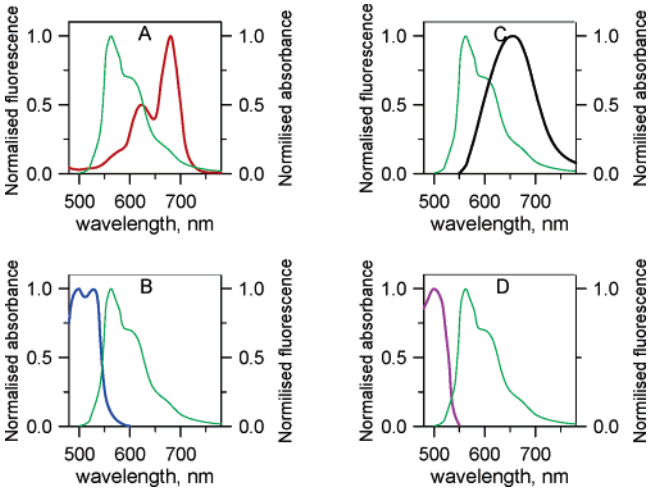

Figure 6. (A) Superimposed absorption spectra of TDI (thick red-color curve) and emission spectra of PI (thin green-color curve) (directional FRET). (B) Absorption (blue color) and emission spectra of PI (green curve) (energy hopping). (C) Transient absorption (S_1-S_n) spectrum (black color) and emission spectra of PI (green curve) (singlet PI−singlet PI annihilation). (D) Transient absorption (S_1-S_n) spectrum of TDI (purple color) and emission spectra of PI (green curve) (singlet PI−singlet TDI annihilation). Spectra were recorded in toluene.[5]

color fluorescence. Indeed, the absolute probability to excite two chromophores for **T2P$_8$** is 3 times higher than that for **T1P$_4$**, and the relative contribution of two-chromophore excitation $P^8{}_2/P^8{}_1$ is approximately twice that of $P^4{}_2/P^4{}_1$. This significant difference should be apparent in experiments as a more frequent appearance of two-color emission for **T2P$_8$** as compared to

TABLE 3: Förster Radii[5]

process	R_0 (nm)
directional FRET	5.9
energy hopping	4.8
singlet (peryleneimide)−singlet (peryleneimide) annihilation	5.3
singlet (peryleneimide)−singlet (terrylenediimide) annihilation	3.7

T1P$_4$. In contrast, the experimental data showed approximately equal contributions of dual-color fluorescence (see Table 4). Furthermore, dual-color fluorescence was observed after bleaching of the majority of donors (see Figure 8). Since the relative contribution of simultaneous excited chromophores reduces when the number of donors decreases (see Table 1), the presence of multiexcitations as a main cause for the appearance of two-color emission is not plausible. This argument is further corroborated by the results of the CW measurements. While multiple chromophores can be excited simultaneously using pulsed excitation, under the same CW excitation power, this probability is extremely low. For example, according to eq 8, the relative contribution of two-chromophore excitation $P^8{}_2/P^8{}_1$ within a 1 ns interval is equal to 0.0063 under a CW excitation power of 2.5 kW/cm^2 (as compared to a value for $P^8{}_2/P^8{}_1$ of 0.42 for the same average power but with pulsed laser light). The percentage of two-color emission detected was found to be almost the same as that for the pulsed excitation case (see Table 4).

Additional evidence against the exciton blockade as the only source of the simultaneous two-color emission can be found by further analyzing the trajectories obtained with pulsed excitation. The arrival times of the photons of trace C from Figure 8 were used to construct the acceptor−acceptor auto-

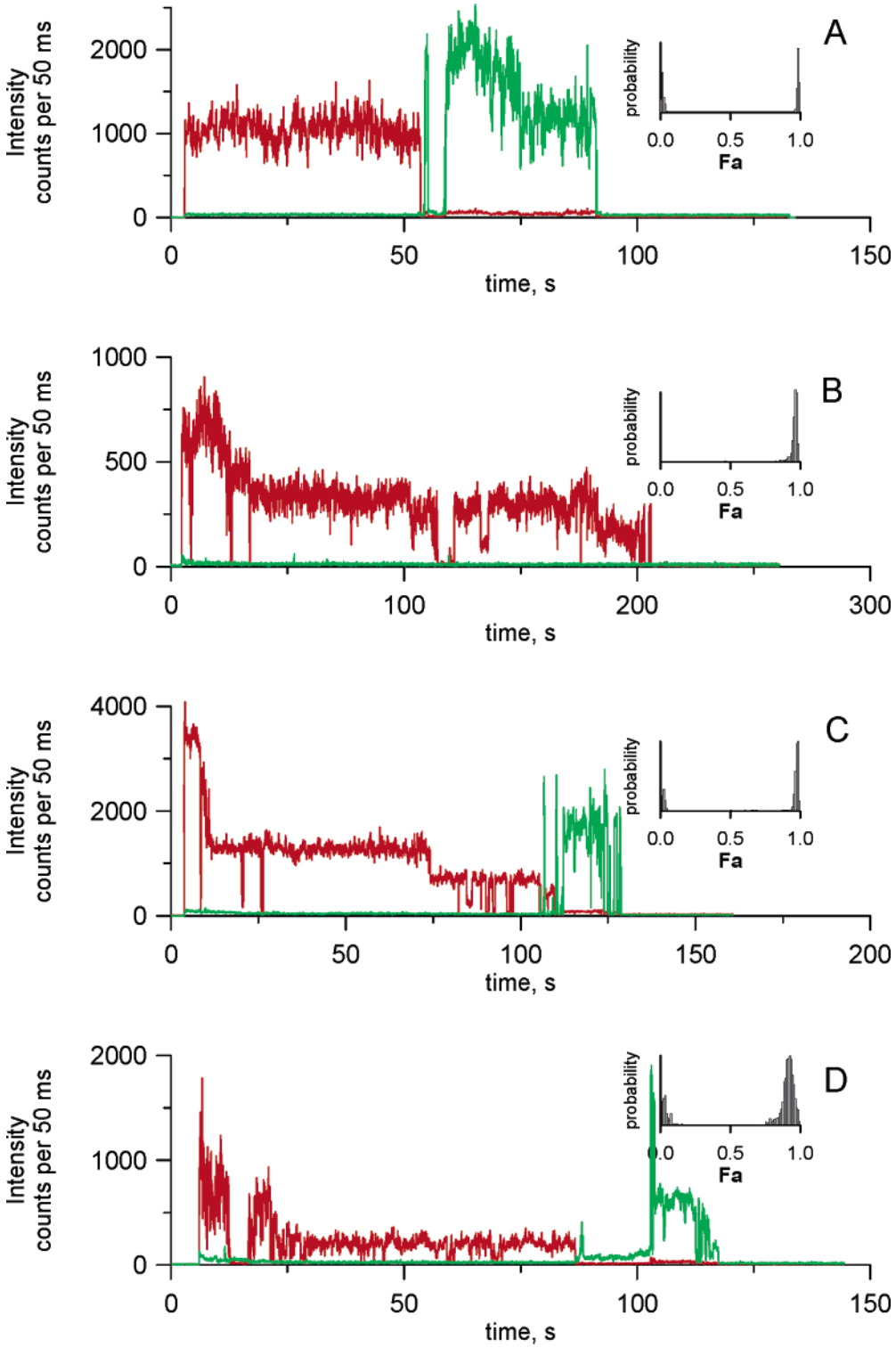

Figure 7. Typical fluorescence transients of single molecules. Red-color and green-color curves denote the acceptor and donor channels, respectively. The insets show the distribution of fractional intensity of the acceptor fluorescence. Parts A and B display **T1P$_4$** molecules, and parts C and D, **T2P$_8$**. Parts A and C correspond to pulse excitation, and parts B and D, to CW excitation.

correlation curve (Figure 9A) and the acceptor−donor cross-correlation curve (Figure 9B).

The zero-peak in the upper histogram (Figure 9A) is much smaller than the adjoining peaks. This indicates that two acceptor detection channels are anticorrelated as expected because only one red emitter (i.e., the acceptor molecule) exists within the dendrimer. The presence of a few events at zero-time is rationalized by signal−background and background−background correlation. The cross-correlation histogram in Figure 9B shows, within statistical deviation, three equal peaks. According to the Monte Carlo simulations, this corresponds to the case of uncorrelated photon sequences (Figure 4B). On the basis of these histograms and simulation results, we can say that the majority of green photons are not positively correlated to red photons. Thus, the presence of multiexcitations cannot solely explain the observed two-color emission phenomenon.

A final piece of evidence consists of the fluorescence decay that can be constructed for the donor emission by histogramming the photon arrival times. From the decay histogram constructed for trace C of Figure 7, a decay time of 4 ns can be obtained.

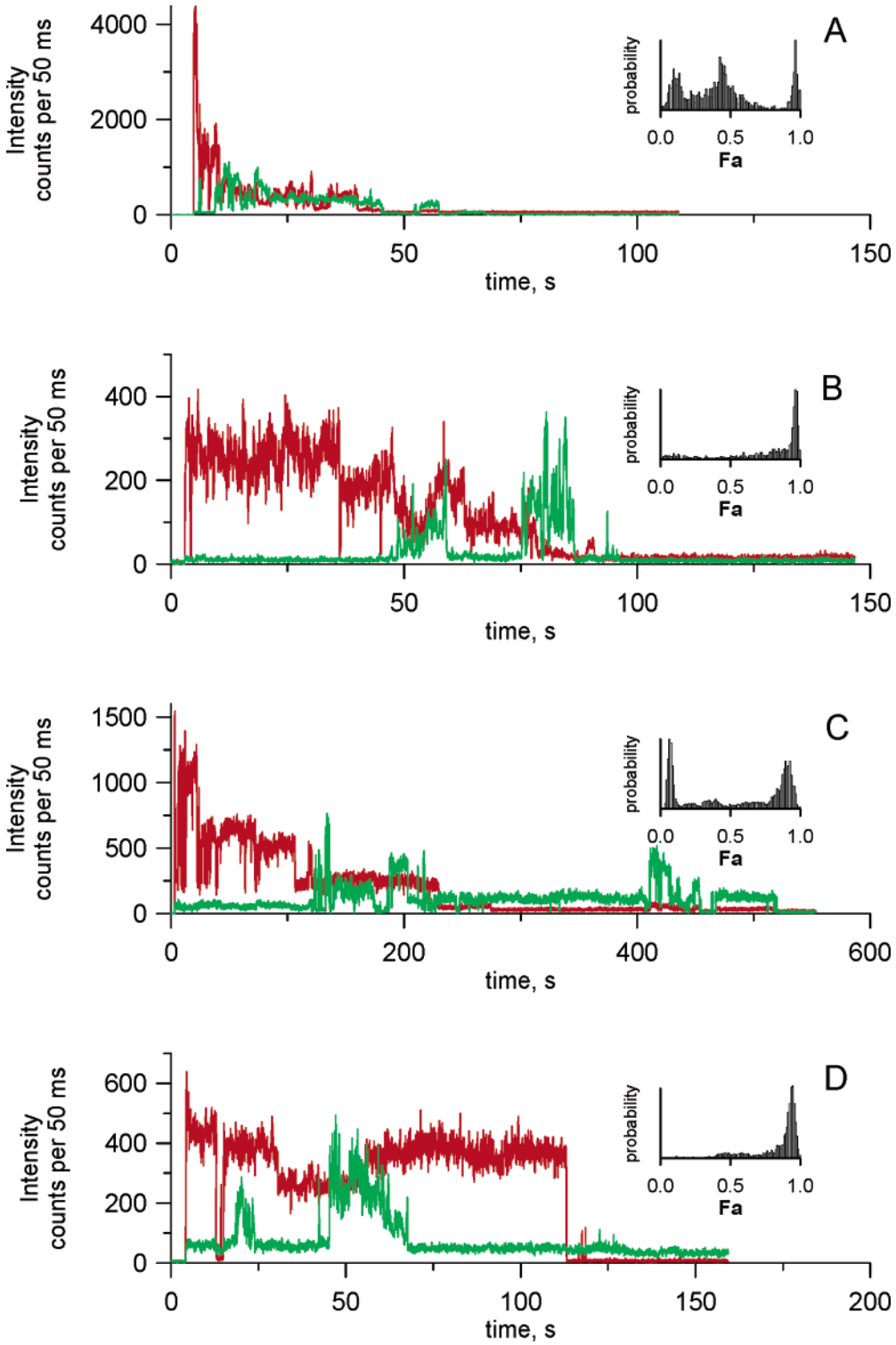

Figure 8. Two-color fluorescence transients of single molecules. Red-color and green-color curves denote the acceptor and donor channels, respectively. The insets show the distribution of fractional intensity of the acceptor fluorescence. Parts A and B display **T1P$_4$** molecules, and parts C and D, **T2P$_8$**. Parts A and C correspond to pulse excitation, and parts B and D, to CW excitation.

This corresponds to the unquenched decay time of the PI chromophore. In the case of an exciton blockade, one expects a partially quenched decay time of PI due to competition of the excited PI to decay via fluorescence ($k_D = 2.5 \times 10^8$ s^{-1}) or via singlet PI−singlet TDI annihilation ($k_{PI-TDIanni} = 4.3 \times 10^9$ s^{-1} (for T1P$_4$) or $k_{PI-TDIanni} = 7.2 \times 10^8$ s^{-1} (for T2P$_8$)). The expected decay times based on these rate constants are 1 ns for the second generation dendrimer and 220 ps for the first generation dendrimer.

TABLE 4: Occurrence of Three Different Modes of Behavior for Single Molecules

			monochromatic emission	
excitation type	compound	two-color emission	only red emission	red followed by green emission
pulse	**T1P$_4$**	12 (11%)	27 (25%)	71 (64%)
	T2P$_8$	51 (15%)	81 (24%)	207 (61%)
CW	**T1P$_4$**	7 (11%)	16 (24%)	43 (65%)
	T2P$_8$	11 (11%)	14 (15%)	70 (74%)

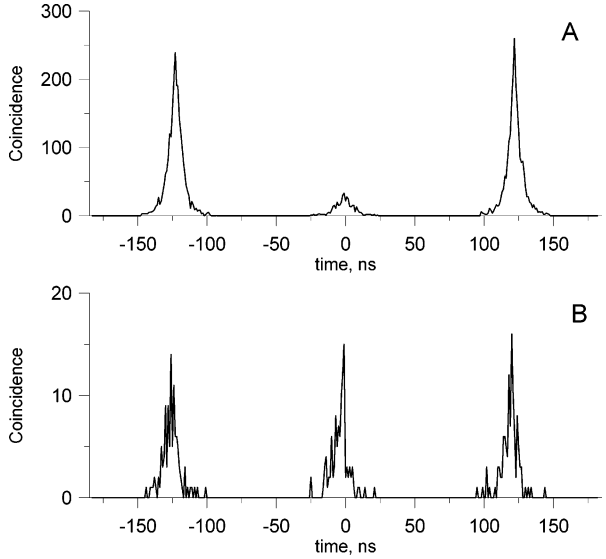

Figure 9. Coincidence histograms taken from the trace displayed in Figure 8C: (upper panel) acceptor autocorrelation; (lower panel) donor−acceptor cross-correlation.

The data presented here form overwhelming evidence that an exciton blockade involving randomly oriented chromophores cannot be the origin of the observed simultaneous donor−acceptor emission. Therefore, another contributing factor must be envisioned that must be related to changes in the energy transfer efficiency. According to the Förster equation, such changes can result either from changes in the spectral overlap or from changes in the orientation factor, κ^2. Spectral data obtained form single molecules show no evidence for large spectral shifts (data not shown). Therefore, we decided to have a closer look at the orientation of chromophores responsible for the simultaneous emission.

4.3. Defocused Wide-Field Imaging. Defocused imaging of single molecules and single nanocrystals has been used to examine the angular distribution of their emission.[22,30,31] We applied this technique to determine the orientation of emitting chromophores in the dendrimers under study. Defocused wide-field image sequences of 45 single **T1P$_4$** molecules and 268 single **T2P$_8$** molecules were recorded by exciting with CW 488 nm light (2.5 kW/cm^2), while detecting donor and acceptor emission on two different cameras. Calibration of the two-camera setup was done in focused wide-field mode with a reference sample. The discrepancy in position along the *x* and *y* axes proved to be within a few pixels.

Figure 10 shows typical defocused images of single dendrimer molecules imbedded in a thin Zeonex film (the upper panels depict **T1P$_4$**, and the lower panels, **T2P$_8$**; the left panels correspond to the red channel, and the right, the green channel). The size of single molecule patterns and the behavior of single molecule fluorescence are practically equivalent for two dendrimer generations. The emission patterns recorded in the red channel (left panels of Figure 10) are noticeably larger than those recorded in the green channel (right panels of Figure 10). This difference in pattern size arises from a wavelength difference between the two detection channels.[31] We note that, within the first 90 s for **T1P$_4$** and 65 s for **T2P$_8$**, only a few dendrimer molecules undergo photobleaching of the acceptor chromophore. Otherwise, the three types of emission (only red, green after bleaching of red, and simultaneous green and red) observed in confocal microscopy can be found back in defocused imaging as well.

Defocused emission patterns of individual acceptor chromophores in the red channel do not vary with time, as expected for one emitter fixed in a polymer film. It also proves that the spatial orientation of the TDI acceptor is fixed relative to the rest of the dendrimer. On the other hand, the defocused emission patterns recorded for some molecules in the green channel display stepwise orientation changes with time. A similar behavior was also observed for a related dendritic system consisting of a tetrahedral polyphenylene core and four PI chromophores at the rim (G1R4).[10] For G1R4, the stepwise changes in orientation were attributed to energy hopping among identical chromophores and emission from an energetically slightly lower trapping site. After bleaching of the first trap, the next chromophore that is lowest in energy will emit, and since its orientation is different, a different pattern will be observed. A similar situation is expected for T1P4 and T2P8 after photodestruction of the acceptor chromophore. The excitation energy migrating between chemically similar donors will be trapped by a donor moiety of the lowest energy. As a result, at any particular time, only one donor chromophore emits. When this donor molecule undergoes photobleaching, another donor molecule will replace it as the next fluorescent trap. Thus, the measured emission pattern displays sequentially different dipole orientations.

The number of dendrimer molecules that display dual-color fluorescence and hence show emission patterns at the same *x*,*y* coordinates in both the green and red channels is comparable to the confocal measurements. Fifteen single dendrimer molecules showing dual-color emission with good signal-to-noise intensity were chosen in order to determine the dipole orientations in both channels. The selected patterns were analyzed using the numerical procedure published before for evaluating dipole orientations.[31] Two examples are illustrated in Figure 11 where each row of images presents individual molecules. The first and second columns correspond to the red-color channel, while the third and fourth represent the green channel. The first and third columns are experimental images, and the second and fourth are the matching simulated patterns.

For the first molecule, the emission dipole of the acceptor chromophore is oriented entirely out of plane (red channel, see Figure 11A and B), while the emission dipole of the donor (very weak signal, image was obtained by integration over an extended time interval) lies in plane (green channel, see Figure 11C and D). The second molecule exhibits both in-plane emission dipoles for the acceptor (Figure 11E and F) and the donor (Figure 11J and H) chromophores, respectively; however, they are both oriented nearly perpendicular to each other. This set of experiments allows for direct visualization of the relative orientation of the emitters responsible for fluorescence in both channels. As a result, one has to re-evaluate the rate constant for FRET and PI−TDI annihilation. These will be substantially different then for the case of randomly oriented chromophores.

The picture that arises from both confocal and wide-field measurements is as follows. In intact dendrimers (no photobleached donor chromophores), energy hopping among the donors ensures that the excitations end up at the acceptor, even if unfavorable oriented donors are present in the dendritic molecule. Multiple excitations within the dendrimer are quenched by a very efficient singlet PI−singlet PI annihilation as well as by important (in comparison with the PI fluorescence decay rate) singlet PI−singlet TDI annihilation which leads to an existence of only one excited chromophore, the acceptor. After photobleaching of a number of donors, unfavorable oriented donors will become "isolated". When these donors are excited, they will not undergo FRET nor will they annihilate with the excited acceptor molecule,[32] eventually populated via other

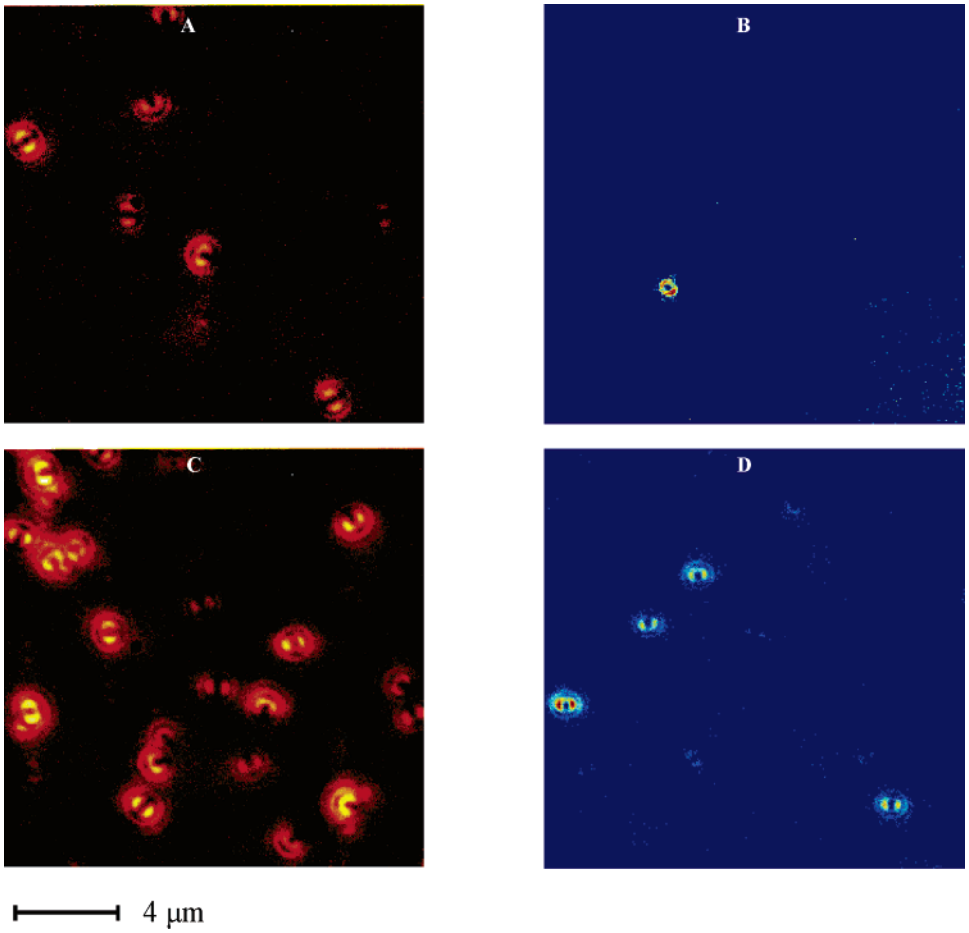

Figure 10. Defocused images of single molecules embedded in a thin polymer film. Parts A and B correspond to **T1P$_4$** molecules, and parts C and D, to **T2P$_8$**. The images were recorded in the time interval 81−90 s for **T1P$_4$** and in the time interval 60−65 s for **T2P$_8$**. The left column corresponds to the acceptor detection channel, and the right column, to the donor detection channel.

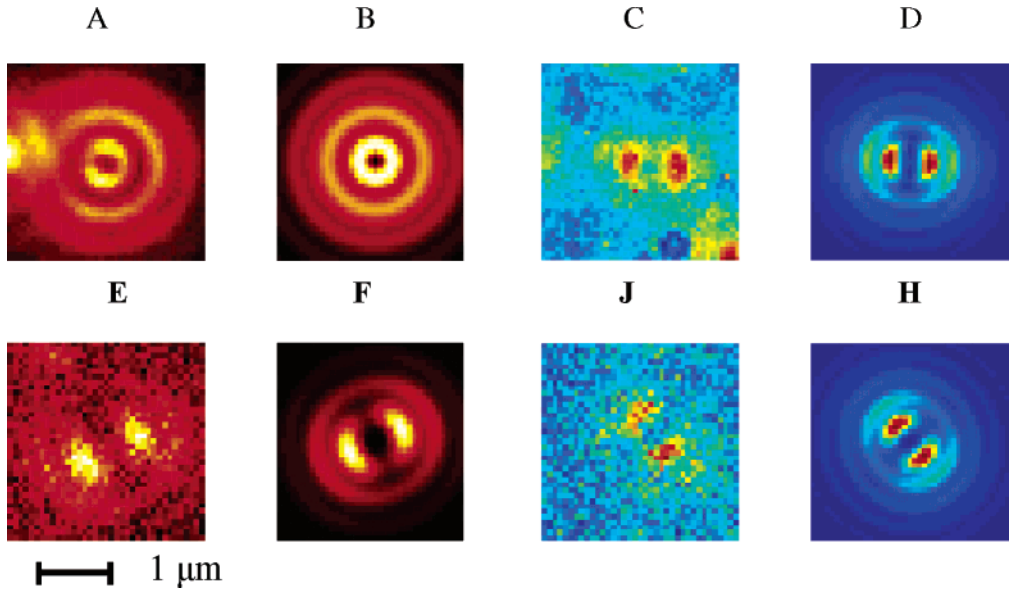

Figure 11. Examples of single **T2P$_8$** molecules which showed dual-color fluorescence. Each row of images presents a different individual molecule. The first and second columns correspond to the red-color channel, and the third and fourth, to the green one. The first and third columns are detected images, and the second and fourth are the matching simulated patterns. The images of the first molecule (A and C) were obtained by integration over several frames; the images in the second row (E and J) correspond to one frame.

donors, but relax to the ground state by emission of fluorescence. Since they are isolated, their decay time has to be identical to that of the PI chromophore, as was observed experimentally. Thus, simultaneous donor−acceptor emission in the dendritic systems studied in this contribution arises mainly from unfavorable oriented donor molecules and only to a minor extent from an exciton blockade resulting from multiple excitations. The question remains of why only a fraction of the molecules show this behavior. We rule out trapped conformations resulting from the spin coating process in the sample preparation due to the

shape persistence of the molecules. In a fraction of the molecules, the unfavorable oriented donor molecules will bleach before the other donor molecules. Most probably though, this observation results from the different conformational isomers that are present in this otherwise chemically identical population of molecules. As pointed out before, the synthetic route leading to the macromolecules under study allows for isomers with different orientations of the PI donor moieties at the rim.[14b,33] The study performed here shows the potential of single molecule spectroscopy to discriminate even such subtle differences in populations of molecules.

5. Conclusions

The phenomenon of dual-color fluorescence in two generations of peryleneimide−terrylenediimide dendrimers has been intensively investigated at the single molecule level. These systems were designed for very fast intramolecular Förster type energy transfer. As a result, most of the single molecules showed green donor emission appearing exclusively after bleaching of the acceptor. However, in an important fraction of the traces (10−15% for different generations and excitation modes), simultaneous green donor and red acceptor fluorescence can be detected.

We have argued by carefully evaluating the ensemble data, by comparing simulated and experimental correlations between the green and red photons, and by changing the excitation conditions that an exciton blockade, resulting from the presence of multiple excitations in the system, and the assumption of randomly oriented donor molecules with respect to the acceptor molecule cannot explain the observed two-color emission. By determination of the spatial orientation of the emitters responsible for the fluorescence in the green and red channels via defocused wide field, we could attribute the observed two-color emission mainly to the presence of an unfavorable oriented donor molecule being present in the system after photobleaching of the majority of suitable oriented donors. If excitations on the acceptor and the donor are present simultaneously in the system, the unfavorable donor is absolutely required to obtain the simultaneous emission in donor and acceptor channels. The hypothesis of a badly oriented donor is consistent with the decay time found for the green emission channel. In the experiments, the importance of the orientation among transition dipoles in Förster type energy transfer processes (both FRET and singlet PI−singlet TDI annihilation) is directly visualized. Finally, it was argued that the relative small fraction of molecules showing the simultaneous emission might be linked to conformational isomers resulting from the synthetic route followed to prepare the dendrimers.

Acknowledgment. The KULeuven research fund (Center of Excellence INPAC, GOA/02/2006), the Federal Science Policy through IAP/V/03, the FWO, and the Laboratory Directed Research and Development (LDRD) program at Los Alamos National Laboratory are acknowledged for supporting this research.

References and Notes

(1) (a) Chen, J.; Li, S.; Zhang, L.; Liu, B.; Han, Y.; Yang, G.; Li, Y. *J. Am. Chem. Soc.* **2005**, *127*, 2165. (b) Puntoriero, F.; Serroni, S.; Galletta, M.; Juris, A.; Licciardello, A.; Chiorboli, C.; Campagna, S.; Scandola, F. *ChemPhysChem* **2005**, *6*, 129. (c) Ceroni, P.; Bergamini, G.; Marchioni, F.; Balzani, V. *Prog. Polym. Sci.* **2005**, *30*, 453. (d) Jiang, D.-L.; Aida, T. *Prog. Polym. Sci.* **2005**, *30*, 403. (e) Suslick, K. S.; Bhyrappa, P.; Chou, J.-H.; Kosal, M. E.; Nakagaki, S.; Smithenry, D. W.; Wilson, S. R. *Acc. Chem. Res.* **2005**, *38*, 283. (f) Wang, B.-B.; Zhang, X.; Jia, X.-R.; Li, Z.-C.; Ji, Y.; Yang, L.; Wei, Y. *J. Am. Chem. Soc.* **2004**, *126*, 15180. (g) Momotake, A.; Arai, T. *Polymer* **2004**, *45*, 5369. (h) Sugiura, K.-I. *Top. Curr. Chem.* **2003**, *228*, 65. (i) Balzani, V.; Ceroni, P.; Maestri, M.; Saudan, C.; Vicinelli, V. *Top. Curr. Chem.* **2003**, *228*, 159. (j) Balzani, V.; Ceroni, P.; Maestri, M.; Vicinelli, V. *Curr. Opin. Chem. Biol.* **2003**, *7*, 657. (k) Maes, W.; Vanderhaeghen, J.; Smeets, S.; Asokan, C. V.; Van Renterghem, L. M.; Du, Prez, F. E.; Smet, M.; Dehaen, W. *J. Org. Chem.* **2006**, *71*, 2987. (l) Loiseau, F.; Campagna, S.; Hameurlaine, A.; Dehaen, W. *J. Am. Chem. Soc.* **2005**, *127*, 11352. (m) Gensch, T.; Hofkens, J.; Herrmann, A.; Tsuda, K.; Verheijen, W.; Vosch, T.; Christ, T.; Basché, T.; Müllen, K.; De Schryver, F. C. *Angew. Chem.* **1999**, *111*, 3970. (n) Dol, G. C.; Tsuda, K.; Weener, J.-W.; Bartels, M. J.; Asavei, T.; Gensch, T.; Hofkens, J.; Latterini, L.; Schenning, A. P. H. J.; Meijer, B. W.; De Schryver, F. C. *Angew. Chem.* **2001**, *113*, 1760. (o) Tsuda, K.; Dol, G. C.; Gensch, T.; Hofkens, J.; Latterini, L.; Weener, J. W.; Meijer, E. W.; De Schryver, F. C. *J. Am. Chem. Soc.* **2000**, *122*, 3445. (p) Dirksen, A.; De Cola, L. *C. R. Chim.* **2003**, *6*, 873. (q) Glazier, S.; Barron, J. A.; Houston, P. L.; Abruna, H. D. *J. Phys. Chem. B* **2002**, *106*, 9993.

(2) (a) Grimsdale, A. C.; Müllen, K. *Angew. Chem.* **2005**, *117*, 5732. (b) Bauer, R. E.; Grimsdale, A. C.; Müllen, K. *Top. Curr. Chem.* **2005**, *245*, 253. (c) Grimsdale, A. C.; Vosch, T.; Lor, M.; Cotlet, M.; Habuchi, S.; Hofkens, J.; De Schryver, F. C.; Müllen, K. *J. Lumin.* **2005**, *111*, 239. (d) Wiesler, U.-M.; Weil, T.; Müllen, K. *Top. Curr. Chem.* **2001**, *212*, 1. (e) Vögtle, F.; Gestermann, S.; Hesse, R.; Schwierz, H.; Windisch, B. *Prog. Polym. Sci.* **2000**, *25*, 987. (f) Gitsov, I.; Lin, C. *Curr. Org. Chem.* **2005**, *9*, 1025. (g) Tomalia, D. A. *Prog. Polym. Sci.* **2005**, *30*, 294. (h) Nantalaksakul, A.; Reddy, D. R.; Bardeen, C. J.; Thayumanavan, S. *Photosynth. Res.* **2006**, *87*, 133.

(3) (a) Maus, M.; Mitra, S.; Lor, M.; Hofkens, J.; Weil, T.; Herrmann, A.; Müllen, K.; De Schryver, F. C. *J. Phys. Chem. A* **2001**, *105*, 3961. (b) Yeow, E. K. L.; Ghiggino, K. P.; Reek, J. N. H.; Crossley, M. J.; Bosman, A. W.; Schenning, A. P. H. J.; Meijer, E. W. *J. Phys. Chem. B* **2000**, *104*, 2596.

(4) (a) Ortiz, W.; Krueger, B. P.; Kleiman, V. D.; Krause, J. L.; Roitberg, A. E. *J. Phys. Chem. B* **2005**, *109*, 11512. (b) Serin, J. M.; Brousmiche, D. W.; Fréchet, J. M. J. *Chem. Commun.* **2002**, *22*, 2605. (c) Adronov, A.; Gilat, S. L.; Frechet, J. M. J.; Ohta, K.; Neuwahl, F. V. R.; Fleming, G. R. *J. Am. Chem. Soc.* **2000**, *122*, 1175. (d) Qu, J.; Liu, D.; De Feyter, S.; Zhang, J.; De Schryver, F. C.; Müllen, K. *J. Org. Chem.* **2003**, *68*, 9802.

(5) (a) Lor, M.; De, R.; Jordens, S.; De Belder, G.; Schweitzer, G.; Cotlet, M.; Hofkens, J.; Weil, T.; Herrmann, A.; Müllen, K.; Van der Auweraer, M.; De Schryver, F. C. *J. Phys. Chem. A* **2002**, *106*, 2083. (b) Jordens, S.; De Belder, G.; Lor, M.; Schweitzer, G.; Van der Auweraer, M.; Weil, T.; Reuther, E.; Müllen, K.; De Schryver, F. C. *Photochem. Photobiol. Sci.* **2003**, *2*, 177. (c) Jordens, S.; De Belder, G.; Lor, M.; Schweitzer, G.; Van der Auweraer, M.; Weil, T.; Herrmann, A.; Wiesler, U.-M.; Müllen, K.; De Schryver, F. C. *Photochem. Photobiol. Sci.* **2003**, *2*, 1118. (d) Schweitzer, G.; Gronheid, R.; Jordens, S.; Lor, M.; De Belder, G.; Weil, T.; Reuther, E.; Müllen, K.; De Schryver, F. C. *J. Phys. Chem. A* **2003**, *107*, 3199.

(6) (a) Cotlet, M.; Gronheid, R.; Habuchi, S.; Stefan, A.; Barbafina, A.; Müllen, K.; Hofkens, J.; De Schryver, F. C. *J. Am. Chem. Soc.* **2003**, *125*, 13609. (b) Liu, D. J.; De Feyter, S.; Cotlet, M.; Stefan, A.; Wiesler, U. M.; Herrmann, A.; Grebel-Koehler, D.; Qu, J. Q.; Müllen, K.; De Schryver, F. C. *Macromolecules* **2003**, *36*, 5918.

(7) (a) Dichtel, W. R.; Hecht, S.; Frechet, J. M. *Org. Lett.* **2005**, *7*, 4451. (b) Weil, T.; Reuther, E.; Müllen, K. *Angew. Chem., Int. Ed.* **2002**, *41*, 1900.

(8) Cotlet, M.; Vosch, T.; Habuchi, S.; Weil, T.; Mullen, K.; Hofkens, J.; De Schryver, F. *J. Am. Chem. Soc.* **2005**, *127*, 9760.

(9) (a) Lor, M.; Jordens, S.; De Belder, G.; Schweitzer, G.; Fron, E.; Viaene, L.; Cotlet, M.; Weil, T.; Müllen, K.; Verhoeven, J. W.; Van der Auweraer, M.; De Schryver, F. C. *Photochem. Photobiol. Sci.* **2003**, *2*, 501. (b) Lor, M.; Thielemans, J.; Viaene, L.; Cotlet, M.; Hofkens, J.; Weil, T.; Hampel, C.; Müllen, K.; Verhoeven, J. W.; Van der Auweraer, M.; De Schryver, F. C. *J. Am. Chem. Soc.* **2002**, *124*, 9918.

(10) Cotlet, M.; Masuo, S.; Luo, G.; Hofkens, J.; Van der Auweraer, M.; Verhoeven, J.; Müllen, K.; Xie, X. S.; De Schryver F. C. *Proc. Natl. Acad. Sci. U.S.A.* **2004**, *101*, 14343.

(11) Petrella, A.; Cremer, J.; De Cola, L.; Bauerle, P.; Williams, R. M. *J. Phys. Chem. A* **2005**, *109*, 11687.

(12) Schryver, F. C.; Vosch, T.; Cotlet, M.; Van der Auweraer, M.; Müllen, K.; Hofkens, J. *Acc. Chem. Res.* **2005**, *38*, 514.

(13) Thompson, A. L.; Ahn, T.-S.; Thomas, K. R. J.; Thayumanavan, S.; Martinez, T. J.; Bardeen, C. J. *J. Am. Chem. Soc.* **2005**, *127*, 16348.

(14) (a) Hofkens, J.; Maus, M.; Gensch, T.; Vosch, T.; Cotlet, M.; Kohn, F.; Herrmann, A.; Müllen, K.; De Schryver, F. *J. Am. Chem. Soc.* **2000**, *122*, 9278. (b) Masuo, S.; Vosch, T.; Cotlet, M.; Tinnefeld, P.; Habuchi, S.; Bell, T. D. M.; Oosterling, I.; Beljonne, D.; Champagne, B.; Müllen, K.; Sauer, M.; Hofkens, J.; De Schryver, F. C. *J. Phys. Chem. B* **2004**, *108*, 16686. (c) Gronheid, R.; Stefan, A.; Cotlet, M.; Hofkens, J.; Qu, J.; Müllen, K.; Van der Auweraer, M.; Verhoeven, J. W.; De Schryver, F. C. *Angew. Chem.* **2003**, *42*, 4209.

(15) Metivier, R.; Kulzer, F.; Weil, T.; Müllen, K.; Basche, T. *J. Am. Chem. Soc.* **2004**, *126*, 14364.

(16) Tinnefeld, P.; Hofkens, J.; Herten, D.-P.; Masuo, S.; Vosch, T.; Cotlet, M.; Habuchi, S.; Müllen, K.; De Schryver, F. C.; Sauer, M. *ChemPhysChem* **2004**, *5*, 1786.

(17) (a) Loos, D.; Cotlet, M.; De Schryver, F. C.; Habuchi, S.; Hofkens, J. *Biophys. J.* **2004**, *87*, 2598. (b) Park, M.; Cho, S.; Yoon, Z. S.; Aratani, N.; Osuka, A.; Kim, D. *J. Am. Chem. Soc.* **2005**, *127*, 15201. (c) Tinnefeld, P.; Sauer, M. *Angew. Chem.* **2005**, *117*, 2698. (d) Hernando, J.; Hoogenboom, J. P.; van Dijk, E. M. H. P.; García-López, J. J.; Crego-Calama, M.; Reinhoudt, D. N.; van Hulst, N. F.; García-Parajó, M. F. *Phys. Rev. Lett.* **2004**, *93*, 236404. (e) García-Parajó, M. F.; Hernando, J.; Mosteiro, G. S.; Hoogenboom, J. P.; van Dijk, E. M. H. P.; van Hulst, N. F. *ChemPhysChem* **2005**, *6*, 819. (f) Sautter, A.; Kaletas, B. K.; Schmid, D. G.; Dobrawa, R.; Zimine, M.; Jung, G.; van Stokkum, I. H. M.; De Cola, L.; Williams, R. M.; Wurthner, F. *J. Am. Chem. Soc.* **2005**, *127*, 6719. (g) Kim, D.; Osuka, A. *Acc. Chem. Res.* **2004**, *37*, 735. (h) Becker, K.; Lupton, J. M. *J. Am. Chem. Soc.* **2006**, *128*, 6468. (i) Barbara, P. F.; Gesquiere, A. J.; Park, S.-J.; Lee, Y. J. *Acc. Chem. Res.* **2005**, *38*, 602. (j) Gesquiere, A. J.; Lee, Y. J.; Yu, J.; Barbara, P. F. *J. Phys. Chem. B* **2005**, *109*, 12366. (k) Yu, J.; Lammi, R.; Gesquiere, A. J.; Barbara, P. F. *J. Phys. Chem. B* **2005**, *109*, 10025. (l) Rybtchinski, B.; Sinks, L. E.; Wasielewski, M. R. *J. Am. Chem. Soc.* **2004**, *126*, 12268. (m) Heilemann, M.; Tinnefeld, P.; Sanchez, Mosteiro, G.; Garcia, Parajo, M.; Van Hulst, N. F.; Sauer, M. *J. Am. Chem. Soc.* **2004**, *126*, 6514.

(18) Gronheid, R.; Hofkens, J.; Kohn, F.; Weil, T.; Reuther, E.; Müllen, K.; De Schryver, F. C. *J. Am. Chem. Soc.* **2002**, *124*, 2418.

(19) In a system with high FRET efficiency, donor emission will occur rarely or not at all. However, for a very strong excitation field, the excitation rate can be large as compared to the acceptor emission rate, and donor absorption may occur when the acceptor is already/still in the excited state. In this situation, which is termed exciton blockade, FRET can not occur, since the acceptor is already excited. Hence, even for a system with high FRET efficiency, donor emission can be seen, provided that the excited state lifetime of the donor is comparable with or shorter than the excited state lifetime of the acceptor. Additionally, no annihilation or quenching of the donor excited state by the accepter excited state should occur for the donor emission to be observed. For a literature example of an exciton blockade, see: Berglund, A.J.; Doherty, A.C.; Mabuchi, H. *Phys. Rev. Lett.* **2002**, *89*, 068101.

(20) Cotlet, M.; Hofkens, J.; Maus, M.; De Schryver, F. C. In *Fluorescence spectroscopy, imaging and probes. New tools in chemical, physical and life sciences*; Kraayenhof, R., Visser, A. J. W. G., Gerittsen, H. C., Eds.; Springer: Heidelberg, 2002; pp 181−224.

(21) Kurtsiefer, C.; Zarda, P.; Mayer, S.; Weinfurter, H. *J. Mod. Opt.* **2001**, *48*, 2039.

(22) Uji-i, H.; Melnikov, S. M.; Beres, A.; Bergamini, G.; De Schryver, F. C.; Hermann, A.; Müllen, K.; Enderlein, J.; Hofkens, J. *Polymer* **2006**, *47*, 2511.

(23) Homemade program developed in a cooperation between the Scientific Software Technologies Center (Belarusian State University) and the Laboratory of Photochemistry and Spectroscopy (Catholic University of Leuven).

(24) Lounis, B.; Moerner, W E. *Nature* **2000**, *407*, 491.

(25) Weston, K. D.; Dyck, M.; Tinnefeld, P.; Müller, C.; Herten, D. P.; Sauer, M. *Anal. Chem.* **2002**, *74*, 5342.

(26) Lippitz, M.; Kulzer, F.; Orrit, M. *ChemPhysChem* **2005**, *6*, 770.

(27) Hanbury-Brown, R.; Twiss, R. Q. *Nature* **1956**, *177*, 27.

(28) Orrit, M. *Single Mol.* **2002**, *3*, 255.

(29) (a) Beveratos, A.; Kühn, S.; Brouri, R.; Gacoin, T.; Poizat, J.-P.; Grangier, P. *Eur. Phys. J. D* **2002**, *18*, 191. (b) Tinnefeld, P.; Weston, K. D.; Vosch, T.; Cotlet, M.; Weil, T.; Hofkens, J.; Müllen, K.; De Schryver, F. C.; Sauer, M. *J. Am. Chem. Soc.* **2002**, *124*, 14310. (c) Zwiller, V.; Aichele, T.; Benson, O. *New J. Phys.* **2004**, *6*, 96. (d) Hübner, C. G.; Zumofen, G.; Renn, A.; Herrmann, A.; Müllen, K.; Basche, T. *Phys. Rev. Lett.* **2003**, *91*, 093903.

(30) (a) Jasny, J.; Sepiol, J. *Chem. Phys. Lett.* **1997**, *273*, 439. (b) Sepiol, J.; Jasny, J.; Keller, J.; Wild, U. P. *Chem. Phys. Lett.* **1997**, *273*, 444. (c) Toprak, E.; Enderlein, J.; Syed, S.; McKinney, S. A.; Petschek, R. G.; Ha, T.; Goldman, Y. E.; Selvin, P. R. *Proc. Natl. Acad. Sci. U.S.A.* **2006**, *103*, 6495. (d) Patra, D.; Gregor, I.; Enderlein, J. *J. Phys. Chem. A* **2004**, *108*, 6836. (e) Schroeyers, W.; Vallée, R.; Patra, D.; Hofkens, J.; Habuchi, S.; Vosch, T.; Cotlet, M.; Müllen, K.; Enderlein, J.; De Schryver, F. C. *J. Am. Chem. Soc.* **2004**, *126*, 14310. (f) Brokmann, X.; Ehrensperger, M.-V.; Hermier, J.-P.; Triller, A.; Dahan, M. *Chem. Phys. Lett.* **2005**, *406*, 210.

(31) Böhmer, M.; Enderlein, J. *J. Opt. Soc. Am. B* **2003**, *20*, 554.

(32) Since the transition dipole for the S_0-S_1 transition is not necessarily the same as the one for the S_1-S_n transition, an excited donor showing an unfavorable orientation for FRET can in principle undergo singlet−singlet annihilation with the excited acceptor. However, since the decay time of the unfavorable oriented donor is exactly the same as that for the donor model compound PI (4 ns), for this particular donor−acceptor dendrimer, changed transition dipole moments are not an issue.

(33) (a) Vosch, T.; Hofkens, J.; Cotlet, M.; Kohn, F.; Fujiwara, H.; Gronheid, R.; Van Der Biest, K.; Weil, T.; Herrmann, A.; Mullen. K.; Mukamel, S.; Van der Auweraer, M.; De Schryver, F. C. *Angew. Chem.* **2001**, *40*, 4643. (b) Vosch, T.; Cotlet, M.; Hofkens, J.; Van der Biest, K.; Lor, M.; Weston, K.; Tinnefeld, P.; Sauer, M.; Latterini, L.; Mullen, K.; De Schryver, F. C. *J. Phys. Chem. B* **2003**, *107*, 6920.